Acta Crystallographica Section A
Foundations of Crystallography
ISSN 0108-7673

Received 13 June 2008
Accepted 13 August 2008

Reliability of Monte Carlo simulations of disordered structures optimized with evolutionary algorithms exemplified with diffuse scattering from $La_{0.70(1)}(Al_{0.14(1)}I_{0.86(1)})$

Thomas Weber,[a]* Arndt Simon,[b] Hansjürgen Mattausch,[b] Lorenz Kienle[c] and Oliver Oeckler[d]*

[a]Laboratorium für Kristallographie, ETH Zürich, Wolfgang-Pauli-Strasse 10, 8093 Zurich, Switzerland, [b]Max-Planck-Institut für Festkörperforschung, Heisenbergstrasse 1, 70569 Stuttgart, Germany, [c]Technische Fakultät, CAU Kiel, Kaiserstrasse 2, 24143 Kiel, Germany, and [d]Department Chemie und Biochemie der Ludwig-Maximilians-Universität, Butenandtstrasse 5-13(D), D-81377 Munich, Germany. Correspondence e-mail: thomas.weber@mat.ethz.ch, oliver.oeckler@cup.uni-muenchen.de

Complex disorder and corresponding diffuse scattering from $La_{0.70(1)}(Al_{0.14(1)}I_{0.86(1)})$ was taken as basis for investigating the reliability, reproducibility and influence of the refinement parameters of evolutionary algorithm refinements of Monte Carlo simulations. Using the same diffuse-scattering data set, a model relying on reasonable *a priori* knowledge about the real structure was used, as well as one that includes no presumptions except the average structure and the chemical composition. To strengthen the complementary character of the approaches, different evolutionary algorithms ('differential' and 'cooperative' evolution) were employed. It was found that the resulting structures are qualitatively and quantitatively in good agreement independent of the strategy used. It is shown that the method of population averaging (applicable only in differential evolution refinements) allows reasonable estimates about uncertainties of structure parameters if proper refinement parameters are chosen, which makes differential evolution the method of choice for quantitative refinements. Recommendations for the best choices of the parameters are given. The disordered structure of $La_{0.70(1)}(Al_{0.14(1)}I_{0.86(1)})$ contains clusters including differently interconnected La_6Al units. The modes of interconnection and local distortions are discussed in detail.

1. Introduction

Two technical advances in the past two decades have opened up new possibilities for the investigation of diffuse scattering and underlying structural disorder. On the one hand, modern area detectors like CCD cameras and image plates not only allow quantitative measurement of diffuse intensities as a matter of routine, but they deliver it (almost) for free as a side product of conventional data collection. Modelling of disorder, on the other hand, strongly benefits from the ever-growing power of computers. Although not fast enough to refine complex structures in a matter of a few minutes, modern computers allow the use of algorithms that seemed ridiculously time-consuming just a few years ago. Qualitative interpretation and simulation of diffuse diffraction patterns are now well established, and Monte Carlo (MC) methods for model building have been described in detail (Welberry & Butler, 1994; Proffen & Neder, 1997; Proffen & Welberry, 1998). There are, however, only a few *quantitative* MC studies based on experimental diffuse data (for a recent review see Welberry & Goossens, 2008). Besides reverse Monte Carlo modelling (McGreevy, 2001), optimization of Monte Carlo models using least-squares methods (Welberry *et al.*, 1998) and evolutionary algorithms (EAs) have been particularly successful for quantitative studies of disorder. Different algorithms have been described and compared (Weber & Bürgi, 2002; Weber, 2005). In contrast to conventional structure refinements on Bragg data, there is little experience regarding the reliability and reproducibility of the results. This raises the question of how robust, accurate and precise results obtained from EAs or MC simulations of disordered structures are. It is far from being clear how structure models are affected by different algorithms, by starting values of parameters, or by parameters of the algorithms themselves, such as mutation or crossover constants. Furthermore, if the aim of a structure determination is a quantitative investigation of disorder and if the methods used are to become routine tools for structural chemists, it is essential to quantify uncertainties.

Currently, there are no established methods for estimating uncertainties obtained from EA/MC refinements. Bürgi *et al.* (2005) have shown that averaging structural information obtained from an EA population not only obtains results faster than taking results from the best individual in a population, but also provides information about the variance of parameters within the population. However, no systematic investigation about the meaning of the variances as a measure for uncertainties was performed. Definition of uncertainties is not only a problem for EA methods but also for least-squares refinements of MC models, even though standard deviations of refined MC model parameters are directly derived by the algorithm. The refined MC parameters, however, are in most cases not the quantities of interest when investigating a disordered material, because they usually represent a simplified, nonphysical and thus hardly transferable energy scheme of interactions. The desired *structural information* is indirectly obtained from the simulated crystal after execution of the MC algorithm. In general, the standard deviations of the refined MC energy parameters cannot be translated to uncertainties about structure parameters like interatomic distances or pair correlation coefficients.

The models used for MC methods often include significant preassumptions about the chemistry of the compound under investigation. Whereas in many cases these can be derived by a broad range of other methods, they rely on experience and intuition in other cases. If robust *a priori* knowledge about the real structure is not available, it is desirable to use nothing but the information from the average structure as a basis for the disorder model. This proves to be most troublesome in cases where the average structure does not contain much chemical information, *i.e.* when a complicated real structure yields a simple average structure.

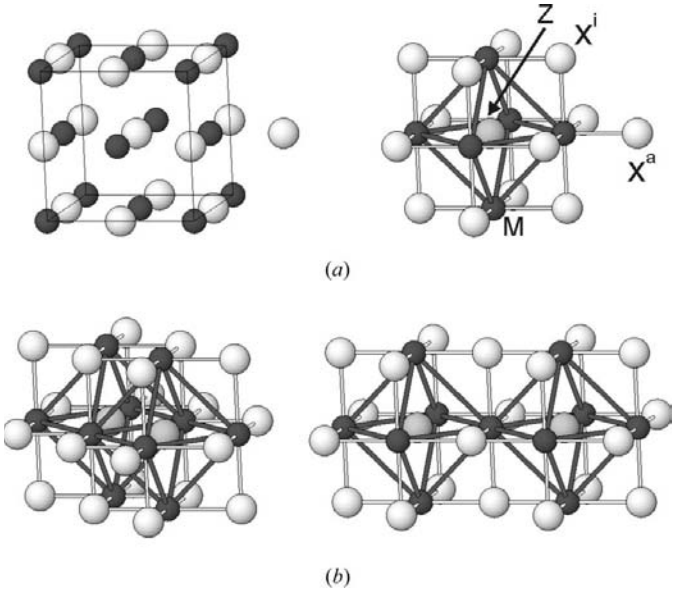

Figure 1
(*a*) Derivation of the $M_6ZX^i_{12}$ cluster (right, with some additional X^a atoms) from the rock-salt structure (left): a Z atom occupying an anion site is enclosed by cationic M atoms forming an octahedron; X^i- and X^a-type atoms are found at next-neighbouring anion sites along ⟨110⟩ and ⟨100⟩ directions, respectively. (*b*) Edge- (left) and corner- (right) sharing condensed clusters (see text).

Recently, we investigated a disordered cluster compound $La_{0.70(1)}(Al_{0.14(1)}I_{0.86(1)})$ with a simple rock-salt type of average structure (Oeckler *et al.*, 2005*a*,*b*). Assuming the presence of well known octahedral La_6Al units, the diffuse scattering (hollow spheres around half of the Bragg reflections, *i.e.* those with odd indices) could be interpreted and used for a quantitative refinement of the clusters' geometry and their relative positions. This compound is an ideal example for comparing results and assessing the reproducibility and reliability of EAs for the refinement of MC models. The short-range-order phenomena are sufficiently complex to evaluate different relatively fine details. Furthermore, optimizing the structure without additional information apart from the approximate overall chemical composition and the Bragg structure poses a significant challenge as the average structure is rather meaningless.

Clusters containing octahedral metal-atom cores are frequently found in metal-rich compounds of early transition metals and in halides of the valence-electron-poor lanthanides. In the latter case, the M_6 octahedron is normally centred by an additional atom Z (*e.g.* B, Al, C, Si and many more like Au) and surrounded by a cuboctahedron of 12 halogen atoms X above all edges. These 'inner' ligands are denoted X^i in order to distinguish them from 'outer' ligands X^a above the six corners of the octahedron.

This cluster configuration is closely related to the rock-salt structure as shown in Fig. 1(*a*). The common close packing of X and Z atoms is complete whereas the cation positions are only occupied around the Z atoms. Increasing the Z/X ratio leads to a condensation of the octahedral units, either *via* corners or *via* edges in case of Z substituting an X^a-type or an X^i-type halogen atom, respectively (Fig. 1*b*). All free edges of the M_6 octahedra are coordinated by X atoms which may belong to only one cluster (X^i) or are shared between clusters with an identical function (X^{i-i}) or a different function (X^{i-a}). Similarly, X^a-type atoms may be shared as X^{a-i} or X^{a-a}-type bridges.

Such cluster compounds represent a large family with many variations in these connectivities (Simon, 1988*a*,*b*; Simon *et al.*, 2006) and they exhibit many interesting structure–property relationships, *e.g.* concerning magnetism (Ryazanov *et al.*, 2006) and superconductivity (Simon *et al.*, 1996). Most of their structures consist of a completely ordered, relatively complex arrangement of clusters within the rock-salt-type basic structure. However, severely disordered representatives are known, such as $Tb_{13}Br_{18}B_3$ (Oeckler *et al.*, 2002*a*,*b*, 2003) with one-dimensional disorder of layers containing pairs of octahedra, or $Ce_{29}Al_{14}I_{28}$ (Oeckler, Mattausch & Simon, 2005) with a more complex short-range order. The compound mentioned above, $La_{0.70(1)}(Al_{0.14(1)}I_{0.86(1)})$, exhibits a much higher degree of disorder than all other rare-earth metal cluster compounds.

The purpose of the present investigation on this compound is to reveal the influence of specific Monte Carlo models,

refinement algorithms and refinement parameters on the structure obtained, and further to estimate the accuracy and precision of the results. From a chemical point of view, it is quite obvious that clusters are present, and without any doubt such *a priori* knowledge should be used in MC models whenever possible. However, in one series of refinements we did not use this information in order to test the ability of the method to find this information. In addition to previous investigations, a more complete diffuse data set was used. To our knowledge, this is the first example of a study where a complete three-dimensional set of diffuse X-ray scattering data was used in a refinement of a complex disorder model that is mostly based on the known average structure and the approximate chemical composition. In order to compare two largely independent approaches to the disordered structure we did not only refine two different MC models, but also used different evolutionary optimization methods.

2. Experimental

The single crystals of $La_{\sim 0.7}Al_xI_{1-x}$ ($x \simeq 0.14$) used in the present study were synthesized from La, LaI_3 and Al mixed stoichiometrically according to a nominal composition La_3I_3Al and heated in a tantalum ampoule at 1148 K for 5 d, resulting in an inhomogeneous sample. Minute variations of the experimental conditions lead to distinctly different products as described in details by Kienle *et al.* (2007). The best method for obtaining pure samples, which usually do not contain good single crystals, is heating a stoichiometric mixture of La, LaI_3 and AlI_3 in a tantalum ampoule at 1148 K for 7 d. The starting materials as well as the product are very moisture sensitive, so all manipulations must be carried out in a glove box or by a Schlenk technique under a purified argon atmosphere. These samples are single phase according to X-ray powder diagrams (using a Stoe Stadi-P diffractometer and Mo K_α radiation). The difficulties posed by the chemical analysis have been discussed by Kienle *et al.* (2007). Energy-dispersive X-ray spectroscopy (EDX) analyses of several macroscopic crystals in a scanning electron microscope (Tescan, Oxford EDX detector) as well as of crystallites in a transmission electron microscope (Philips CM30/ST, Noran Si/Li EDX detector, Vantage System) confirm the given composition, but are not very precise (see below). Elemental analysis on bulk samples is precise; however, compounds with similar but slightly different compositions exhibit almost the same strong reflections in powder patterns so it is ambiguous whether the sample really consists exclusively of crystallites with the same diffuse scattering in their diffraction patterns.

X-ray diffraction data from a single crystal were collected using Ag K_α radiation and a MAR345 image-plate detector. The full 345 mm diameter of the image plate was read out with a pixel size of 150 µm. The crystal-to-detector distance was 170 mm, the oscillation range was 0.5° per frame and the exposure time was 900 s per frame. Altogether 492 frames were collected from the randomly oriented crystal, which was mounted in a glass capillary.

The program package *XCAVATE* (Estermann & Steurer, 1998) was used for the reconstruction of an undistorted three-dimensional volume of reciprocal space. Data were corrected for polarization effects and geometric factors. The diffuse data used as a basis for all refinements described in this paper covered a complete volume ranging from $h, k = 0, \ldots, 6$ and $l = 0, \ldots, 3.9$ and are therefore more complete than the data used in Oeckler *et al.* (2005*a*,*b*). The dimension of a single voxel was 0.1 reciprocal lattice units in each direction, *i.e.* the refinement was based on $61 \times 61 \times 40 = 148\,840$ voxels.

To obtain accurate intensities up to $2\theta = 70°$, Bragg reflections were measured on an Enraf–Nonius CAD-4 four-circle diffractometer using Mo $K\alpha$ radiation. A complete data set of half a sphere was recorded and numerically corrected for absorption effects based on the crystal shape after optimizing the distances and inclination of faces based on ψ-scan data (Stoe & Cie, 1999, 2002). There was no need for a decay correction.

3. Average structure

As the average structure of $La_{0.70(1)}(Al_{0.14(1)}I_{0.86(1)})$ is a simple rock-salt type [$|\mathbf{a}| = 6.323$ (1) Å], there is only marginal direct or indirect information on the complex real structure. The La atoms (cations) and I/Al atoms (anions) of the rock-salt type occupy one Wyckoff position each. However, the data fit is significantly improved when small offsets of the La and I atoms from the ideal rock-salt positions are allowed. Owing to the high symmetry, this yields multiple split positions. The precise probability density around the nodes of the rock-salt lattice cannot be determined unambiguously; however, the best fit is obtained if an octahedral 'split atom cluster' of (0, 0, z) positions is used. Apart from a scale factor, the resolution-dependent gradients of the form factors of La, I and Al are not sufficiently different to allow for a distinction of the elements if partial occupancies must be taken into account. Even precise low- and high-angle diffraction data do not distinguish a partially occupied I-atom site from a fully occupied Al site, for example. As the overall electron density correlates with the scale factor, the only information about element concentrations directly accessible from Bragg data is the ratio of electron densities at the La and I/Al positions. As the only reasonable atom distribution involves La atoms on the partially occupied cation site and a mixture of I and endohedral (and thus anionic) Al on the anion site, three occupancy factors (La, Al, I) are needed for describing the average structure. Obtaining them *ab initio* is impossible, as only a single value (ratio of electrons on the cation site to electrons on the anion site) can be determined. There is no known cluster compound derived from a basic rock-salt type exhibiting vacancies in the anion lattice. Therefore it can be assumed that the occupancies of Al and I add up to 1. However, one more piece of information is necessary to determine three occupancy factors. In previous refinements we assumed that octahedral La_6Al units are rarely interconnected *via* common La atoms and thus the occupancy of the La sites is approximately six times that of Al. However,

Table 1
Results of refinements of the average structure assuming different La/I ratios within the error limits of chemical analyses.

Given molar ratio La/I	Fraction of Al on anion site (cluster concentration)	Chemical formula (occupancies)	Percent of La atoms belonging to two clusters†	*R*1, *wR*2‡
0.730§	0.064	$La_{0.69}Al_{0.06}I_{0.94}$	none, and additional La atoms that are not part of clusters	0.0292, 0.066
0.740	0.111	$La_{0.66}Al_{0.11}I_{0.89}$	<0.1	0.0292, 0.066
0.742	0.120	$La_{0.66}Al_{0.12}I_{0.88}$	5.3	0.0292, 0.066
0.744	0.130	$La_{0.65}Al_{0.13}I_{0.87}$	20.5	0.0292, 0.066
0.746	0.140	$La_{0.64}Al_{0.14}I_{0.86}$	30.7	0.0292, 0.065
0.750	0.157	$La_{0.63}Al_{0.16}I_{0.84}$	49.4	0.0292, 0.065
0.760§	0.198	$La_{0.61}Al_{0.20}I_{0.80}$	94.2	0.0292, 0.066

† Assuming the presence of La_6Al clusters and that no La atom can belong to three clusters. ‡ $R1 = \sum |F_o - F_c| / \sum |F_o|$, $wR2 = \{\sum[w(F_o^2 - F_c^2)^2] / \sum[w(F_o^2)^2]\}^{1/2}$, $w = 1/[\sigma^2(F_o^2) + (aP)^2 + bP]$ with $P = [\max(0, F_o^2) + 2F_c^2]/3$. § Values for comparison: outside error limits of typical analyses, but obtained in single measurements (probably affected by artefacts).

this assumption is just a rough approximation and cannot be used if the purpose is to compare results that are not based on assumptions about the mode of connection or even the existence of clusters. The most reliable experimental result is the molar ratio La/I obtained by EDX analyses (the small content of the light element Al cannot be determined with a comparable accuracy). If a certain ratio is used as a constraint, all occupancies can be determined. Should clusters be present, their degree of interconnection is related to the molar ratio La/Al obtained in a constrained refinement. Taking into account uncertainties in the experimentally obtained La/I ratio, we performed a series of refinements with different ratios in a range consistent with the experimental findings. Table 1 shows the refined concentration of Al on the anion site, obtained under the constraint of several La/I ratios compatible with the chemical analysis. Even slight variations within the error limits of EDX analyses (or bulk analyses of compounds that may contain small impurities) yield extremely strong variations in the degree of cluster condensation. This means that for refinements based on Bragg data the given La/I ratio has a strong influence on the possible degree of cluster condensation in the unit cell. On the other hand, the deviation of the split positions from the ideal rock-salt-type positions does not significantly depend on the La/I ratio assumed. It is 0.25 (1) Å for La and 0.22 (1) Å for I. The Al site was not affected by split positions.

4. Observations and qualitative interpretation

The most striking diffuse feature in the diffraction pattern is a system of hollow spheres, which are only present around Bragg reflections with *h*, *k*, *l* = all odd (Fig. 2). The global symmetry of the diffuse intensities follows the $m\bar{3}m$ Laue symmetry of the Bragg reflections, which means that the interactions and thus the correlations between the disordered species follow the high symmetry of the average structure. The radius of the spheres is about 0.1 $Å^{-1}$, *i.e.* about 0.7|**a***|. The half-width of the skins of the spheres along radial directions is approximately 0.05 $Å^{-1}$ or 0.3|**a***|. To a first approximation, the spheres may be understood as representing an isotropic short-range-ordered modulation with a modulation vector of length ~10 Å and a correlation length of about 20 Å. The existence of spherical modulations in the real structure may be explained by local attractive forces and medium-range repulsive forces due to strain in the crystal structure introduced by the local attractions as shown by Welberry (2001) for the two-dimensional case. From a diffractionist's point of view, the existence of diffuse scattering only around positions *h*, *k*, *l* = all odd in rock-salt-like structures is an indication of the presence of anti-phase domains, where neighbouring domains are shifted relative to each other by vectors $\langle\frac{1}{2}00\rangle$. When different domains host the same elements and cover the same volume, the local rock-salt structure becomes primitive cubic on average with half the lattice constant of the local face-centred-cubic cell. Consequently, reflections with *h*, *k*, *l* = all odd become extinct and, depending on the ordering of the domains, they are replaced by diffuse or sharp satellite scattering. The distance of these features from the extinct reflections corresponds to the extent of typical domain–anti-domain sequences. Reflections *h*, *k*, *l* = all even are not affected by anti-phase domain disorder since they represent a superposition of anion- and cation-site properties, which are insensitive to $\langle\frac{1}{2}00\rangle$ displacements and therefore they also show no satellite intensities. From a chemical point of view, however, anti-phase domains are not possible in the present structure, because anti-phase domain boundaries would certainly not be stable. This discrepancy can be resolved by the following considerations. Assuming that all Al atoms are fully enclosed by La_6 octahedra, all voids must be enclosed by I_6 octahedra. Consequently, both anion and cation sites host similarly shaped units having a weak scatterer (V^{La}/Al) in the centre that is enclosed by six strong scatterers (I/La). Not from chemical properties, but from positions and relative scattering power, single La_6Al and I_6V^{La} units may to a good approximation be understood as anti-phase (micro-)domains. Assuming a preference for undirected alternations of La_6Al and I_6V^{La} [*e.g.* for arrangements along ⟨111⟩, see Fig. 3 in Oeckler *et al.* (2005*a*,*b*)], which both have a size of approximately 6 Å in diameter, one would expect an isotropic short-range-ordered anti-phase superstructure with a modulation vector length of about 12 Å, *i.e.* diffuse spheres around reflections *h*, *k*, *l* = all odd having a radius of about

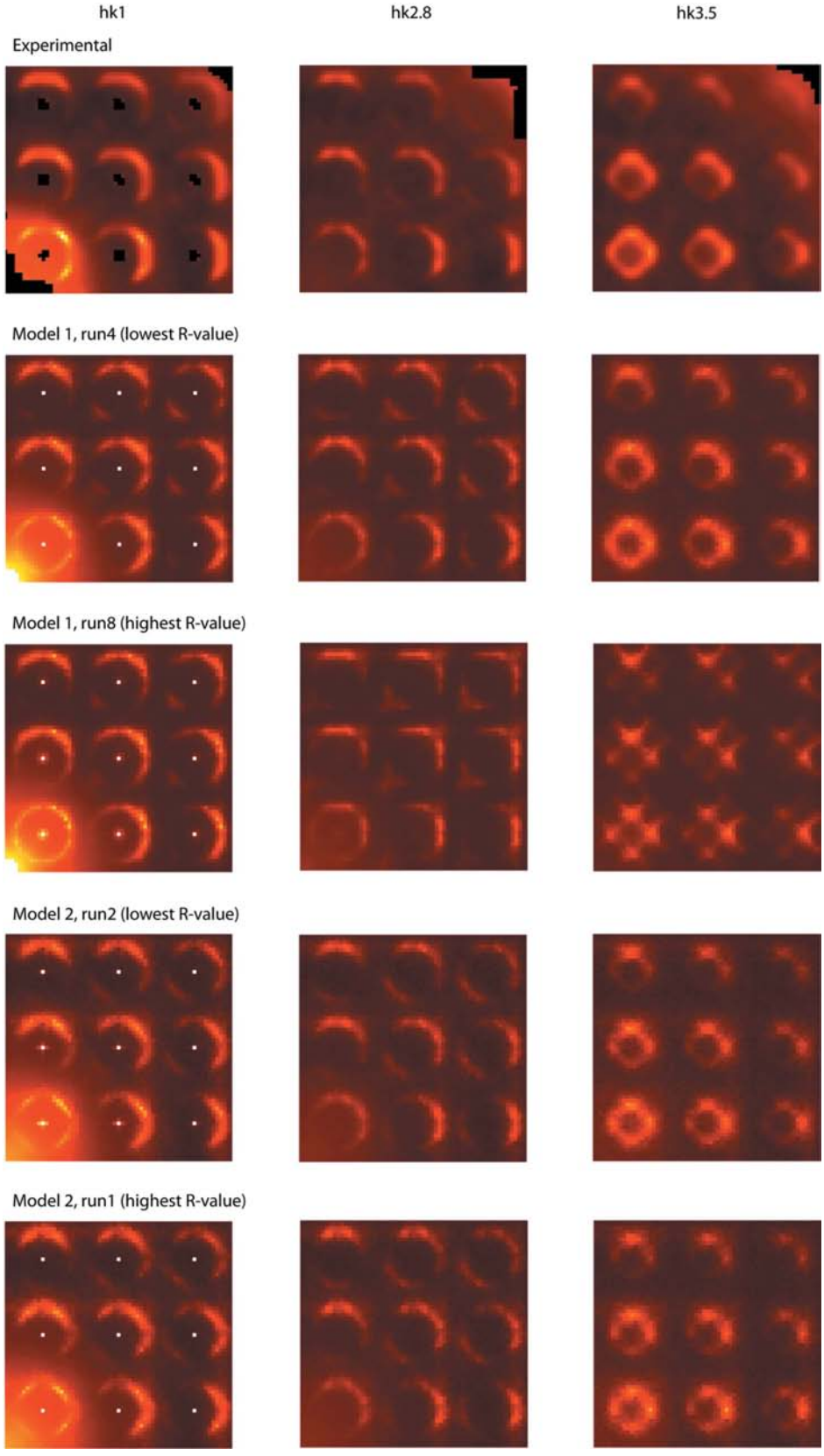

Figure 2
Comparison of the experimental diffraction pattern with calculated intensities from model 1 and model 2 for layers *hk*1, *hk*2.8 and *hk*3.5. For each model the calculated diffraction patterns with highest and lowest *R* values are shown. Unsatisfactory results for run 8 can clearly be identified by comparing the diffraction patterns. Black areas in the experimental data indicate regions that were excluded from the refinement because they represent Bragg reflections or strong parasitic background scattering. The sections range from $h, k = 0, \ldots, 6$ with $h = k = 0$ being at the lower left corner of the images.

1/12 Å^{-1}. This estimate is in a good agreement with the experimental findings. The fact that reflections h, k, l = all odd are not extinct may be explained by the differences in concentration and scattering power of La_6Al and I_6V^{La} units. In general, the intensity distribution on the spheres is highly asymmetric. The intensities are strong on the high-angle side of each sphere and weak or even absent on the low-angle side. This observation indicates a so-called size effect (Welberry & Butler, 1994), *i.e.* displacements correlated with substitutional disorder of differently sized, or, as is more generally said, differently shaped structural units. Consequently, environment-dependent displacements have to be considered in the models.

The maxima seen on the cross sections of the spheres are actually arc-shaped modulations of the diffuse intensities, which indicates that the modulations responsible for the existence of the diffuse spheres are not completely isotropic. This intensity modulation is strong on spheres close to the origin of reciprocal space, but less pronounced on spheres at high scattering angles. Other diffuse scattering is found beneath strong Bragg reflections. The intensities of these phenomena are weak and the location and the shape of these intensities suggest that it is most probably thermal diffuse scattering (TDS). Since we will focus on structural disorder, TDS-like scattering was eliminated from the diffraction data before starting the refinement.

5. Modelling and refinement

As a consequence of the uncertainties in the average structure mentioned above, two series of refinements were carried out which rely on information from the average structure to a different degree. Model 1 is mostly based on crystal-chemical *a priori* knowledge and uses only a little information from the average structure. In contrast, model 2 is strictly constrained to the results from the average structure refinements and does not depend on any structural preassumptions about local order–disorder phenomena. The goal of the second series was to have an independent crosscheck of the results obtained by model 1 and to elucidate whether it would be possible to derive the complicated real structure refined in model 1 without using *a priori* assumptions about local arrangements. To further strengthen the complementary character of the refinements, models 1 and 2 were optimized using two different optimization methods. Model 1 was refined with the differential evolution (DE) method (Weber & Bürgi, 2002; Price & Storn, 1997), while the second model was optimized using the cooperative evolution (CE) technique (Weber, 2005). To test the reproducibility as well as robustness against variations of refinement parameters and uncertainties in the average structure, refinements were repeated several times with different refinement parameters.

5.1. Model 1

5.1.1. The crystal model. Model 1 is essentially the same as the one described by Oeckler *et al.* (2005*a*,*b*), but it is explained in more detail in the following. Structure building was done in four steps. In the first step, only the spatial arrangement of the clusters was simulated using Al atoms as representatives for complete clusters. The simulation was initialized by distributing Al atoms randomly on anion sites according to the occupation factor o(Al), which was also refined by DE to possibly account for uncertainties in the chemical analysis. At this stage, all cation sites as well as anion sites not occupied by Al were left empty. The distribution of Al atoms and thus the distribution of the clusters was obtained using an Ising-model-like MC simulation. A randomly selected Al atom was moved to another also randomly selected but void anion site and the energy difference before and after the move was calculated according to the change of the atom's environment. The potential of a site i occupied by Al was calculated by $E_i = \sum_j \sigma_{ij} J_{ij}$, where the summation runs over all j neighbouring anion sites within a distance smaller or equal to the length of the direct space vector $(2\frac{1}{2}\frac{1}{2})$, which was found by trial and error. The interaction parameter σ_{ij} is +1 if site j is also occupied by Al and −1 if it is empty, while J_{ij} are interaction energies between octahedral units i and j to be refined by DE. Symmetry-equivalent interatomic vectors according to the Laue symmetry $m\bar{3}m$ were given the same J_{ij} values. Since it has rarely been observed (and is unlikely except in layered compounds) that an La atom is connected to three clusters, this configuration was suppressed by giving a constant penalty energy of $E = 50kT$ to configurations having more than two Al atoms next-neighboured to the same cation site. A move was accepted with a probability $p_{\rm accept} = \exp(-\Delta E)/[1 + \exp(-\Delta E)]$, where ΔE is the energy difference (in multiples of $1/kT$) resulting from the move. The simulation was repeated over 200 cycles, where one cycle is defined such that every Al in the structure is considered once on average. In the second step, the structure was completed in a deterministic way by filling all cation sites next to an Al atom with La and all void anion sites with I. Cation sites not occupied by La were left empty. Consequently, the average occupation factor of I is obtained by o(I) = 1 − o(Al), while the number of La atoms present in the crystal is a function of the frequency of edge and corner sharing in clusters. In the hypothetical case that all La_6Al units are isolated, the total number of La atoms is exactly six times the number of Al atoms. Each corner-sharing contact of octahedra reduces the total number of La atoms in the structure by one and each edge-sharing condensation reduces the total number of La atoms in the structure by two. The influence of the degree of cluster connections on the relative concentration of La and Al may be calculated by $o(\mathrm{La})/o(\mathrm{Al}) = 6 - 2c_{\rm e} - c_{\rm c}$, where $c_{\rm e}$ and $c_{\rm c}$ are the average number of edge- and corner-sharing connections per octahedron, respectively. The third step was introducing displacive distortions by moving La atoms as well as $X^{\rm i}$- and $X^{\rm a}$-type I atoms along radial directions relative to the centres of the corresponding clusters. The quantity of the displacement was governed by one parameter for each of the three kinds of displacements, the signs and magnitudes of which are subject to the DE refinement. All influences of single clusters were summed up in the case of corner- or edge-

sharing configurations, *i.e.* an La atom was not shifted if connecting two octahedra *via* corners, while in the case of edge-sharing configurations the atoms move along the La–La connection line (*cf.* Fig. 3). Analogous rules were applied to displacements of I atoms occupying X^{i-i}, X^{i-a} or X^{a-a} positions of more than one cluster. In the final step, all atoms were randomly displaced according to a common isotropic mean-square displacement factor U_{uncor} to account for uncorrelated displacements. This last step is the only difference to the model used in Oeckler *et al.* (2005*a*,*b*). In summary, this model requires 15 structure parameters to be optimized.

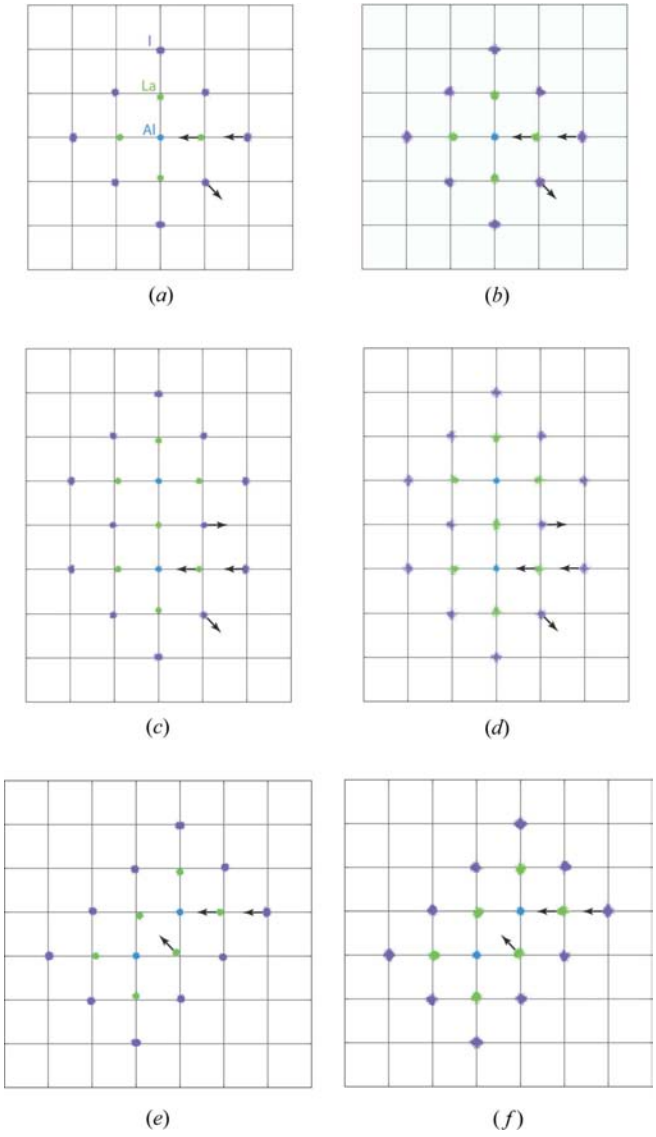

Figure 3
Scatter plots of cross sections through isolated clusters (*a*, *b*), corner-sharing clusters (*c*, *d*) and edge-sharing condensations (*e*, *f*). The left column shows superpositions of clusters from run 1 in model 1, while the plots in the right column are taken from run 1 in model 2. Scatter plots from other refinements give comparable results. The nodes of the gridlines, which have a spacing of $|\mathbf{a}|/2$, represent the ideal sites of the rock-salt structure. Arrows indicate characteristic displacements from the rock-salt structure nodes. In model 1 only the magnitudes and the signs of the displacements are refined, while the respective directions are restricted by the MC model. In model 2 displacements are unrestrained.

5.1.2. Calculation of intensities. To reduce statistical noise from the calculated intensities, a method originally introduced by Butler & Welberry (1992) was used. The final crystal structure was subdivided into equally sized lots each containing $10 \times 10 \times 10$ unit cells, *i.e.* a lot covered $63.2 \times 63.2 \times 63.2$ Å. Each lot is therefore significantly larger than the disorder correlation length of about 20 Å (see §4), as is required for avoiding artefacts due to too-small lot sizes. The Fourier transform of each lot was calculated and the intensities of all lots were summed up incoherently.

For a comparison of observed and calculated diffuse intensities, a proper scale factor and a background model are required. The total intensity was calculated using

$$I_{calc}(\mathbf{h}) = aI_{calc,0}(\mathbf{h}) + b + c|f_{Si}(d\mathbf{h})|^2, \quad (1)$$

where $I_{calc,0}$ are intensities as obtained from the Fourier transform of the structure using the lot mechanism described above, a is a scale factor and b is a constant background contribution. As the shape of the background resembles typical profiles of atomic form factors, the variable part of parasitic scattering was simulated using $f_{Si}(\mathbf{h})$ as a prototypic model. The intensity of the variable background is scaled by c and its width by d. Note that the choice of the silicon form factor as a model for the background is arbitrary and justified only because it gave satisfying results and implementation of the technique was straightforward. The parameters a, b and c were obtained directly by a linear least-squares fit. Parameter d cannot be obtained by the linear least-squares method and was therefore included as an additional parameter in the DE refinement.

5.1.3. The differential evolution refinement. A comprehensive description about the optimization of MC models using DE is found in Weber & Bürgi (2002). Parameters required for a DE refinement are the crossover constant f_r, the mutation constant f_m and the population size p, which all have to be provided by the user. Our refinements were done with f_r and f_m having the values 0.6 and 0.8 in all four possible permutations. We tried two variants for finding new individuals. In the so-called *elitist* mode, one parent of a new child is always the best individual found so far, *i.e.* the search space for finding parameter values for genes of a new individual is restricted to the environment of the current 'leader', while in the *non-elitist* mode all individuals may be selected as new parents with the same probability. The elitist mode is expected to converge faster than the non-elitist mode but has a higher risk of a premature loss of genetic diversity and thus getting stuck in a local minimum. The number of individuals per population was 80 in all cases, *i.e.* more than five times the number of refined parameters. The size of the crystal was n^3 lots with $n = 1, 2, 3, \ldots$. Each run was started with one lot and n was incremented if no child was replacing a parent during one generation. There is no general stop criterion for EA refinements. Bürgi *et al.* (2005) have shown that the essential structural information from their DE/MC refinements may be obtained by averaging the information from a population after some ten generations, while consecutive generations mainly have the effect of reducing noise in the calculated diffraction

patterns. It is therefore reasonable to stop a refinement at the latest if increasing the lot number (= reducing statistical noise) has no significant influence on the R values and on the refined parameters over several generations. This termination criterion was applied in this study, although the refinements are therefore more time consuming compared to stopping at an earlier stage and relying on population averages as proposed by Bürgi *et al.* (2005). Between 3 and 20 CPUs on a cluster of Macintosh G5 2 GHz computers were available for parallel computing. Since the available computing power was strongly fluctuating even during one refinement it is difficult to report the total CPU time consumed. The total wall-clock time required for one run was between five and ten days.

The start values of all Ising parameters J_{ij} describing the distribution of the clusters were taken randomly from a range $-1kT$ to $1kT$, the shift parameters describing local relaxations were taken from −0.22 to 0.22 Å, while initial values o(Al) were chosen from the interval 0.11 to 0.14 and start values for uncorrelated displacements ranged from 0 to 0.05 Å^2. Reflecting boundary conditions were applied to restrict the possible parameter values ('world size') of o(Al) to between 0.10 and 0.15 and $U_{\rm uncor}$ to between 0 and 0.1 Å^2. All other parameter values were unrestrained.

5.2. Model 2

5.2.1. The Monte Carlo model. In contrast to model 1, model 2 is (almost) exclusively based on information from the average structure, *i.e.* neither information about the existence of clusters nor preassumptions about local relaxations are included. This generalization introduces additional degrees of freedom and therefore refinement of model 2 is significantly more challenging than that of model 1. For the initialization of the MC model, anion sites of the rock-salt structure were randomly filled by Al or I atoms corresponding to the respective average occupancy parameters. The atoms were then randomly displaced in accordance with the split displacements and anisotropic displacement parameters from the average structure. Analogously, cation sites were randomly filled by La atoms. The vacancies were represented as pseudo-atoms $V^{\rm La}$ with no displacements. The MC simulation was done by swapping atoms between anion and cation sites such that the average structure was unaffected by the MC simulation (Proffen & Welberry, 1998). Again, the change of the total energy induced by the manipulation of the structure was calculated and the modification was accordingly accepted or rejected as described above.

The energy of a site i was calculated assuming an Ising model and Hooke's spring interactions with the six next-neighbouring atoms, *i.e.* $E_i = \sum_{j=1}^{6} k_{ij}(d_{ij} - d_{0,ij})^2 + J_{ij}$, where d_{ij} is the distance between the atoms in the simulated crystal, while $d_{0,ij}$ (the equilibrium position of Hooke's potential), k_{ij} (the force constant) and J_{ij} (Ising parameter) are parameters to be found for each of the next-neighbour pairs La–I, La–Al, $V^{\rm La}$–Al and $V^{\rm La}$–I. To reduce the number of parameters as well as correlations, which were strongly affecting the performance of early trials, constraints J_{ij}(La–I) = $-J_{ij}$(La–Al) and $J_{ij}(V^{\rm La}\text{–I}) = -J_{ij}(V^{\rm La}\text{–Al})$ were used, which were found as a trend in initial tests. As a consequence of the computational complexity of model 2, it was not possible to find a complete interaction scheme by trial and error as usually done when setting up an MC model. Pair interactions beyond next-neighbour correlations were taken from model 1, *i.e.* Ising-model-like Al–Al interactions up to a distance corresponding to a vector $(2\frac{1}{2}\frac{1}{2})$ were employed. Adopting this interaction scheme provides information about the length of medium-range Al interactions; however, no bias towards formation of La_6Al units or towards special local relaxation rules is introduced. In all cases pair-interaction parameters were constrained to obey Laue symmetry $m\bar{3}m$. Altogether, model 2 has 20 MC parameters.

5.2.2. The cooperative evolution refinement. The CE method was described in detail by Weber (2005). Contrary to DE, where each individual builds its own crystal, all individuals of a CE population cooperate in building *one* model crystal. Further, in contrast to DE, CE is not generation-based, and it does not aim to converge to a relatively homogenous population, but it allows strong genetic diversity even if the model has converged to a homogenous structure. The parameters of the refinement are a mutation constant $f_{\rm m}$ and a parameter $f_{\rm t}$ that controls selection pressure and population size p. Owing to its higher complexity, the refinement of model 2 was extremely time consuming, which did not allow testing of the influence of variations of $f_{\rm m}$, $f_{\rm t}$ and p. Again, the lot mechanism as described above was used for calculating diffraction intensities. The (constant) crystal size was 40 × 40 × 40 unit cells subdivided into 64 lots each containing 10 × 10 × 10 unit cells. Determination of scale and background factors was done analogously to model 1 using equation (1). To accelerate the refinement, the background parameter d from equation (1) was not refined but taken as a constant from the results of model 1. As shown in Table 1, small uncertainties in element concentrations may have a strong impact on some aspects of the real structure. In contrast to model 1, the concentration of elements is defined at the beginning of an evolutionary refinement and not changed afterwards. To account for the uncertainty of the element occupations, four refinements were done with o(Al) = 0.11, 0.12, 0.13 and 0.14. The concentration of I was calculated as o(I) = 1 − o(Al), while o(La) as well as displacement parameters were taken from the average structure (Table 1). The start values for the Ising parameters J_{ij} were randomly chosen from the range $\pm 1kT$ in all cases. The spring parameters k_{ij} were chosen from 0 to 100 $kT/|\mathbf{a}|^2$ and the initial equilibrium distances $d_{0,ij}$ ranged from 2.84 to 3.48 Å. Force constants k_{ij} were restrained to have positive values and the world size for each J_{ij} was between $-100kT$ and $100kT$. Equilibrium distance parameters $d_{0,ij}$ were allowed to vary between 1.83 and 5.48 Å.

The CE refinement was parallelized by distributing the calculations to 14 nodes of a Macintosh cluster. Owing to intrinsic properties of the CE algorithm, parallelization is not as efficient as it is in the case of DE, *i.e.* efficiency was only about 60%, compared to about 95% for DE refinements. Refinements were stopped if no significant improvement of

Table 2
Results from the refinements of model 1.

For each run the results from the best individual (left-hand column of each pair) as well as the average and the e.s.d.'s from all individuals within the corresponding population (right-hand column of each pair) are shown.

	Run															
	1		2		3		4		5		6		7		8	
Mode	elitist		elitist		elitist		elitist		non-elitist		non-elitist		non-elitist		non-elitist	
Individuals	80		80		80		80		80		80		80		80	
f_r	0.6		0.8		0.6		0.8		0.6		0.8		0.6		0.8	
f_m	0.6		0.6		0.8		0.8		0.6		0.6		0.8		0.8	
Lots	64		64		125		125		64		64		125		64	
Generations	241		228		280		304		245		325					
Average structure																
o(La)	0.72	0.716 (7)	0.60	0.598 (7)	0.67	0.66 (3)	0.71	0.70 (2)	0.69	0.66 (4)	0.70	0.67 (3)	0.57	0.63 (4)	0.58	0.58 (9)
o(I)	0.85	0.8505 (6)	0.88	0.882 (2)	0.87	0.875 (7)	0.86	0.863 (6)	0.86	0.86 (1)	0.86	0.857 (5)	0.89	0.87 (1)	0.89	0.87 (1)
o(Al)	0.15	0.1494 (6)	0.12	0.117 (2)	0.13	0.125 (7)	0.14	0.137 (6)	0.14	0.14 (1)	0.14	0.142 (5)	0.11	0.13 (1)	0.11	0.13 (1)
U_{iso}(La) (Å^2)	0.10	0.103 (3)	0.11	0.108 (3)	0.09	0.10 (1)	0.08	0.078 (7)	0.13	0.10 (2)	0.10	0.10 (2)	0.13	0.11 (4)	0.10	0.13 (7)
U_{iso}(I) (Å^2)	0.05	0.051 (3)	0.02	0.021 (1)	0.05	0.049 (7)	0.06	0.056 (6)	0.05	0.04 (2)	0.04	0.036 (1)	0.02	0.04 (1)	0.01	0.05 (3)
U_{iso}(Al) (Å^2)	0.02	0.020 (2)	0.00	0.0003 (4)	0.03	0.026 (6)	0.03	0.025 (3)	0.01	0.008 (5)	0.01	0.010 (6)	0.01	0.009 (6)	0.01	0.01 (1)
Spatial cluster correlations																
$\langle\frac{1}{2}\frac{1}{2}0\rangle$	0.59	0.60 (2)	0.66	0.65 (2)	0.45	0.46 (5)	0.49	0.49 (6)	0.62	0.6 (1)	0.62	0.7 (1)	0.61	0.7 (1)	0.44	0.8 (4)
$\langle100\rangle$	0.32	0.30 (5)	0.00	0.003 (2)	0.05	0.06 (3)	0.18	0.17 (7)	0.26	0.3 (2)	0.22	0.3 (1)	0.16	0.4 (2)	0.32	1 (1)
$\langle1\frac{1}{2}\frac{1}{2}\rangle$	0.77	0.77 (3)	0.59	0.60 (2)	0.88	0.84 (8)	0.87	0.87 (8)	0.73	0.8 (2)	0.75	0.7 (2)	0.46	0.6 (1)	0.79	0.7 (5)
$\langle110\rangle$	1.05	1.06 (4)	1.16	1.15 (4)	1.07	1.1 (3)	1.08	1.1 (1)	1.12	1.1 (4)	1.10	1.1 (3)	1.36	1.0 (3)	0.62	1 (1)
$\langle\frac{3}{2}\frac{1}{2}0\rangle$	1.37	1.36 (2)	1.45	1.46 (2)	1.43	1.41 (7)	1.38	1.38 (5)	1.38	1.4 (1)	1.33	1.4 (1)	1.61	1.5 (2)	1.87	1.5 (5)
$\langle111\rangle$	1.61	1.61 (7)	1.75	1.77 (7)	1.53	1.6 (3)	1.49	1.5 (2)	1.61	1.7 (6)	1.63	1.8 (5)	1.82	1.7 (2)	2.06	2 (1)
$\langle\frac{3}{2}1\frac{1}{2}\rangle$	1.15	1.15 (2)	1.25	1.25 (1)	1.12	1.15 (7)	1.12	1.12 (7)	1.21	1.2 (1)	1.19	1.2 (1)	1.15	1.2 (1)	1.18	1.2 (5)
$\langle200\rangle$	0.66	0.67 (8)	0.64	0.66 (8)	0.54	0.7 (2)	0.60	0.6 (1)	0.55	0.6 (6)	0.72	0.8 (5)	0.77	0.5 (3)	0.23	1 (1)
$\langle\frac{3}{2}\frac{3}{2}0\rangle$	0.73	0.72 (2)	0.62	0.62 (3)	0.74	0.75 (8)	0.76	0.77 (7)	0.73	0.7 (2)	0.81	0.8 (2)	0.55	0.6 (2)	0.65	0.8 (7)
$\langle2\frac{1}{2}\frac{1}{2}\rangle$	0.96	0.96 (2)	0.95	0.94 (2)	1.00	1.00 (6)	1.02	1.03 (5)	0.98	1.0 (1)	0.98	1.0 (2)	0.83	1.0 (1)	0.83	1.1 (5)
$\langle210\rangle$	0.90	0.90 (1)	0.93	0.94 (1)	0.88	0.86 (5)	0.83	0.85 (4)	0.90	0.9 (1)	0.88	0.9 (1)	1.00	1.0 (1)	0.85	1.2 (8)
Isolated clusters (%)	4.50	5 (1)	18.20	19 (2)	32.64	31 (9)	17.68	19 (9)	6.30	10 (8)	5.90	5 (3)	22.6	8 (19)	36.3	7 (7)
Average next-neighbour distances (Å)																
Al–La	2.91	2.912 (5)	2.86	2.859 (3)	2.92	2.92 (2)	2.96	2.95 (1)	2.85	2.90 (4)	2.89	2.90 (2)	2.84	2.89 (4)	2.88	2.89 (8)
La–I	3.28	3.285 (4)	3.28	3.297 (2)	3.27	3.27 (1)	3.27	3.269 (7)	3.31	3.29 (2)	3.28	3.29 (1)	3.30	3.30 (2)	3.25	3.31 (5)
I–V^{La}	3.08	3.080 (4)	3.10	3.103 (2)	3.10	3.102 (6)	3.08	3.082 (8)	3.07	3.08 (2)	3.09	3.10 (1)	3.12	3.09 (2)	3.14	3.10 (4)
Distances within isolated clusters (Å)																
Al–La	2.89	2.896 (4)	2.85	2.854 (4)	2.92	2.91 (2)	2.95	2.94 (1)	2.83	2.89 (4)	2.88	2.88 (2)	2.83	2.87 (5)	2.87	2.58 (9)
La–I^i	3.25	3.253 (4)	3.25	3.257 (3)	3.25	3.25 (1)	3.25	3.251 (8)	3.28	3.27 (3)	3.26	3.26 (2)	3.24	3.27 (2)	3.22	3.28 (5)
La–I^a	3.33	3.340 (7)	3.39	3.393 (4)	3.32	3.33 (2)	3.29	3.30 (2)	3.38	3.36 (5)	3.33	3.36 (3)	3.45	3.38 (6)	3.36	3.42 (1)
R value	0.077	0.0780 (2)	0.081	0.0811 (2)	0.076	0.0768 (4)	0.0757	0.0761 (1)	0.081	0.083 (1)	0.079	0.0814 (6)	0.085	0.091 (2)	0.094	0.099 (2)

the structure could be observed over 100 h. Owing to the complexity of the model, the structure was computationally much more demanding then model 1, *i.e.* the complete execution of one refinement took about two months.

6. Results and discussion

6.1. General

Fig. 2 shows the layers $hk1$, $hk2.8$ and $hk3.5$ as obtained by refinements of models 1 and 2 compared to the experimental data. The layers are taken from the best individuals of runs 4 and 8 from model 1 and runs 2 and 1 from model 2, *i.e.* from the runs with the lowest and highest R values in each case, where $R = [\sum(I_{obs} - I_{calc})^2 / \sum I_{obs}^2]^{1/2}$. Except for run 8 of model 1, all patterns show a satisfying agreement between observations and calculations. The principal features of the experimental diffuse intensities are nicely reproduced: diffuse spheres with proper radius are observable at expected positions and local maxima as well as intensity asymmetries regarding the centres of the spheres are also found to a good approximation. In agreement with the experiment, no diffuse spheres are found around reflections with h, k, l = all even.

The statistical evaluation of the results is shown in Tables 2 and 3. In Table 2, which shows the results for model 1, the best individual within a population as well as the corresponding population averages including their estimated standard deviations (e.s.d.'s) are given. In Table 3 the results of model 2 are reported, as well as the averages and e.s.d.'s of all $7 \times 80 = 560$ individuals from runs 1–7 of model 1 and runs 1–4 of model 2. Note that CE refinements do not allow the calculation of meaningful population averages. As seen in Table 2, the R values of the refinements in elitist mode are slightly smaller than those of the non-elitist refinements. The smaller

Table 3
Results from the refinements of model 2, and a comparison of the averages and e.s.d.'s of all individuals from model 1 (excluding run 8, which did not converge) and all runs of model 2.

	Run				Average model 1 (runs 1–7)	Average model 2 (runs 1–4)
	1	2	3	4		
Individuals	120	120	120	120		
f_m	0.5	0.5	0.5	0.5		
f_t	0.9	0.9	0.9	0.9		
Average structure (not refined by CE)						
o(La)	0.659	0.652	0.649	0.644	0.66 (4)	0.651 (6)
o(I)	0.89	0.88	0.87	0.86	0.87 (1)	0.87 (1)
o(Al)	0.11	0.12	0.13	0.14	0.14 (1)	0.12 (1)
U_{iso}(La) (Å^2)	0.084	0.084	0.084	0.084	0.10 (2)	0.084
U_{iso}(I) (Å^2)	0.085	0.085	0.085	0.085	0.04 (1)	0.085
U_{iso}(Al) (Å^2)	0.030	0.030	0.030	0.030	0.01 (1)	0.03
Cluster correlations						
$\langle\frac{1}{2}\frac{1}{2}0\rangle$	0.530	0.663	0.792	0.793	0.6 (1)	0.7 (1)
$\langle100\rangle$	0.140	0.091	0.107	0.064	0.2 (2)	0.10 (3)
$\langle1\frac{1}{2}\frac{1}{2}\rangle$	0.700	0.847	0.851	0.866	0.7 (1)	0.82 (8)
$\langle110\rangle$	1.270	1.093	1.176	1.198	1.1 (2)	1.18 (7)
$\langle\frac{3}{2}\frac{1}{2}0\rangle$	1.330	1.368	1.410	1.365	1.4 (1)	1.37 (3)
$\langle111\rangle$	1.740	1.731	1.741	1.669	1.6 (3)	1.72 (4)
$\langle\frac{3}{2}1\frac{1}{2}\rangle$	1.160	1.210	1.270	1.260	1.2 (1)	1.22 (5)
$\langle200\rangle$	0.930	0.800	0.910	0.900	0.6 (3)	0.89 (6)
$\langle\frac{3}{2}\frac{3}{2}0\rangle$	0.500	0.650	0.800	0.750	0.7 (2)	0.7 (1)
$\langle2\frac{1}{2}\frac{1}{2}\rangle$	1.070	1.110	1.130	1.100	1.0 (1)	1.10 (2)
$\langle210\rangle$	0.870	0.960	1.000	1.020	0.9 (1)	0.96 (7)
Isolated clusters (%)	33.900	22.978	11.701	9.463	13 (11)	20 (11)
Isolated La atoms (%)	14.700	11.226	9.092	5.024	—	10 (4)
La atoms belonging to more than two clusters (%)	0.140	0.360	0.800	0.800	<0.01	0.5 (3)
Next-neighbour distances (Å)						
Al–La	2.970	2.973	2.990	2.992	2.91 (3)	2.98 (1)
La–I	3.270	3.281	3.281	3.286	3.29 (2)	3.280 (7)
I–V^{La}	3.060	3.074	3.076	3.077	3.09 (1)	3.072 (8)
Next-neighbour distances within isolated clusters (Å)						
Al–La	2.940	2.941	2.958	2.966	2.89 (3)	2.95 (1)
La–I^i	3.270	3.275	3.274	3.280	3.26 (2)	3.275 (4)
La–I^a	3.330	3.325	3.318	3.314	3.35 (4)	3.322 (7)
o(La) at position next to Al (%)	96.400	93.798	96.053	95.052	—	95 (1)
R value	0.079	0.077	0.078	0.077	0.081 (5)	0.078 (1)

standard deviations of R values and structure parameters and the closer relation between the best individual and the population average indicate that the elitist-mode runs converged better (but not necessarily to better results, see below) than non-elitist refinements. The R values of model 2 are comparable to those of the elitist refinements of model 1. The variation of the structure parameters obtained by model 1 and 2 is small and the results are consistent (for a detailed discussion about the results see below) except for run 8 of model 1. As this run has not only the highest R values, but also a bad qualitative agreement with the experimental diffraction pattern and large e.s.d.'s for R values and structure parameters, we conclude that this run did not converge. The bad performance of run 8 can be explained by the corresponding refinement parameters. This run was executed in non-elitist mode, and it has the largest values for the crossover and mutation constants, *i.e.* it has the largest search space for better solutions and consequently convergence is slow. On the other hand, run 1 from model 1 has the smallest search space and thus the e.s.d.'s of the structure parameters are the smallest of all runs. Taking the average of all individuals from runs 1–7 of model 1 (Table 3) as the best guess for the true values, we find that elitist-mode refinements tend to underestimate the uncertainties, *i.e.* the variation of the values between the runs ('outer variance') is larger than the e.s.d.'s within a population ('inner variance'), while non-elitist refinements overestimate them. The most consistent results, *i.e.* values that agree within three e.s.d.'s with the average of all individuals, were found for runs 3–6, which are also the runs with the lowest R values within the groups of elitist/non-elitist refinements. It may therefore be assumed that the e.s.d.'s of the average of runs 1–7 of model 1 are also overestimated, because averaging includes sub-optimum runs (1, 2 and 7), which have a stronger impact on the e.s.d.'s than the mean values of the respective parameters. Interestingly, the most successful elitist-mode runs 3 and 4 have large mutation constants f_m, while these are small in the best non-elitist-mode runs 5 and 6. A large mutation constant therefore seems to

compensate for the effect of the intrinsically small search space in elitist refinements and, *vice versa*, the intrinsically large search space due to using the non-elitist mode is successfully repressed by a small mutation constant. On the contrary, small mutation constants in the elitist mode lead to a rapid loss of genetic diversity and thus to nicely converged but sub-optimum results with e.s.d.'s that are too small, while large f_m values in non-elitist mode prohibit convergence within a reasonable time. As far as was tested in this study, the variation of the crossover constant f_r seems to have a less distinct influence on the performance of the refinements. The present results do not allow a definite conclusion about the role of this parameter in DE/MC refinements to be drawn.

Although it has a higher degree of freedom, model 2 does not yield significantly lower R values than model 1. This may be explained by the differences in the underlying MC models. A cluster occupying an energetically disadvantageous position in model 2 can only move to a more favourable place if it is deconstructed step-by-step at its old position and reconstructed at the new position. At advanced stages of the refinement, energy parameters strongly favour complete clusters and, consequently, a high energy barrier has to be overcome when deconstructing a cluster and therefore reaching equilibrium becomes very slow. In contrast, repositioning clusters in model 1 is fast, because clusters are implicitly moved as complete units.

6.2. Average structure

The average structures obtained from model 1 are not restricted to results from the Bragg refinement, but result from the refined MC model. The properties of the average structure directly depend on the refined disorder with the only restriction being that the Al occupancy factor is restrained to values between 0.10 and 0.15. As seen in Table 2, the refined Al concentration shows some preference for $o(\mathrm{Al}) \simeq 0.13$–$0.14$; however, the bandwidth of the results covers almost the complete world size of $o(\mathrm{Al})$ and therefore no definite conclusion can be drawn about the total cluster concentration. The same is true for refinements of model 2 (Table 3), where no preference for a specific Al concentration can be observed. The strong variation in the occupancy of La in model 1 is, as expected, strongly correlated with the variation of the Al occupancy and therefore also a consequence of uncertainties in the element concentrations. Comparing the refined occupancies of model 1 with those shown in Table 1, we find that at least the population averages of runs 3–7 and the average of runs 1–7 are consistent with the results of the Bragg structure. Runs 1 and 2 do not yield fully satisfying results when understanding the e.s.d.'s as standard uncertainties.

The displacement parameters U_{iso} shown in Tables 2 and 3 are calculated as the mean-square displacements from the ideal anion and cation sites of the NaCl structure, *i.e.* they include information about local relaxations (split positions) and about thermal or random displacements. The displacement parameters of model 1 are in a good agreement with the average structure (= U_{iso} of model 2, see Table 3) apart from $U_{iso}(\mathrm{I})$, which is significantly smaller than the reference values from model 2. The average structure of model 2 was restrained to the Bragg structure and not modified by the CE refinement; no further analysis is therefore required.

6.3. Cluster correlations

The correlation coefficients shown in Tables 2 and 3 represent the ratio of the total number of observed cluster pairs for given vectors $\langle uvw \rangle$ relative to a completely random distribution. Correlation-coefficient values smaller (larger) than 1 mean that the corresponding pairs are present with smaller (higher) frequency than in the case of a random distribution. The population averages of model 1 and the results of model 2 give consistent results with relatively small e.s.d.'s. Consistent with the findings by Oeckler *et al.* (2005*a*,*b*), edge- and in particular corner-sharing configurations are less favourable than a random distribution of La_6Al units. The frequency of edge-sharing configurations is about 2/3 of a random distribution, while corner-sharing configurations are rare or possibly do not even exist. Strongest correlations are found between units separated by vectors $\langle \frac{3}{2}\frac{1}{2}0 \rangle$ and $\langle 111 \rangle$, *i.e.* by about 10 and 11 Å, respectively, which nicely correlates with the radius of the diffuse spheres (~1/10 $\mathrm{Å}^{-1}$). Consistent with the approximate half-width of the skins of the diffuse spheres (~1/20 $\mathrm{Å}^{-1}$), only weak correlations beyond 15 Å are present. The $\langle 111 \rangle$ correlation means a void V^{La} between the clusters which allows for relaxation of I atoms, *i.e.* they can move towards the void and thus take the optimum distance to La atoms of the clusters.

The fraction of isolated La_6Al octahedra, *i.e.* those that are not connected to other La_6Al octahedra, shows a strong variation from about 4 to 34% of all octahedra and it is strongly correlated with the variance of the Al concentration. This can be understood from the fact that the probability of having all 18 next-neighbouring anion sites (12 *via* edges and 6 *via* corners) of the La_6Al units unoccupied by other octahedra strongly decreases with increasing Al concentration. In both series the fraction of La atoms belonging to more than two octahedra is negligibly small (<1%). While this behaviour was enforced in model 1 by a large penalty term, it was found by model 2 without external bias.

6.4. Next-neighbour distances

Al–La distances of the real structure are smaller compared to average next-neighbour cation–anion distances (3.162 Å), while I–La contacts are longer. If next-neighboured to a vacancy, I atoms move towards the voids by about 0.1 Å relative to the ideal sites of the rock-salt structure. The scatter plots shown in Fig. 3 represent a superposition of single clusters and of dimers with edge- or corner-sharing configurations as taken from the model crystal. The scatter plots of model 1 and 2 give essentially the same information. Compared to the average position, it is consistently found that La and Al atoms move along radial directions relative to the centres of clusters. In both models, displacements of La and I atoms, which belong to two octahedra, may to a good

approximation be described as the sum of the influences caused by the individual clusters. While the direction of local relaxations was enforced by model 1, it was found by model 2 without *a priori* chemical information. In general, interatomic distances between specific pairs of atoms were found with an accuracy significantly better than 0.1 Å.

6.5. Completeness of clusters

Model 1 enforces the formation of complete La_6Al units and therefore perfection of the clusters requires no testing. The crucial parameter for testing the completeness of clusters in model 2 is the occupancy of La sites next-neighboured to Al. In the case of having perfect clusters only it is expected to be 1, while, for instance, in the case of a random distribution of Al and La the environment of Al is expected to be filled by La with the occupancy factor of the average structure, *i.e.* by about 2/3. Table 3 shows that about 95% of the sites next to Al were found to be filled by La and thus the condition for perfect clusters is not completely fulfilled. This result is not necessarily to be interpreted such that the crystal structure hosts incomplete clusters in a significant number. As discussed above, it is expected that at the final stage of the simulation rearrangement of clusters is slow and accompanied by cluster fragments, even if MC parameters strongly favour building of complete clusters. It has been shown by Weber (2005) that pair-correlation probabilities of 1 can hardly be reproduced with current MC simulation techniques, but are usually a few percent smaller than 1. Another indication that the assumption of complete clusters is consistent with the refinements is that model 1, which hosts complete clusters only, gives fits which are comparable or even better than those of model 2.

Unexpectedly (but not impossible) from a chemical point of view, a significant number of La atoms in model 2 are located on sites not next-neighboured to Al positions. An explanation for this observation may be given by the following considerations. Analogously to the finding of incomplete clusters, slow equilibration of the MC model may also be the reason why a fraction of the La atoms, which are supposed to be next to Al, are found at isolated positions. Further, the ratio o(Al)/o(La) obtained by Bragg refinement is constant during CE modelling, but the initial concentrations do not necessarily match the requirements of the refined cluster connectivity. For instance, in run 1 the ratio o(Al)/o(La) = 1/6, which may only be correct if there is no corner- or edge-sharing condensation. Our refinements, however, show that at least edge-sharing configurations are clearly present in the structure, *i.e.* the presumed average structure is not compatible with the real structure in every detail.

7. Conclusions

The two series of refinements of the disordered structure of $La_{0.70(1)}(Al_{0.14(1)}I_{0.86(1)})$ using complementary Monte Carlo models and optimization methods gave consistent qualitative and quantitative structural results. The results are chemically reasonable and consistent with the findings reported by Oeckler *et al.* (2005*a*,*b*). It was found that corner-sharing configurations of La_6Al units are, if any, present in only a small number, while edge-sharing configurations are found significantly more often, but with lower frequency than expected for a random distribution of clusters. The strongest correlations are between clusters separated by vectors ⟨111⟩. La atoms and outer ligands of single-octahedron clusters move along a radial direction towards the Al atoms, while the inner ligands move away from the cluster's centre. If atoms belong to more than one cluster, displacements can be described as the sum of the influences from corresponding clusters whereby each cluster behaves to a good approximation like an isolated cluster. Comparison of the results from models 1 and 2 show that the assumptions about the existence of clusters and local relaxations made in model 1 can also be reproduced without using this information explicitly in the MC model 2. Somewhat more ambiguous results were obtained regarding the *absolute* number of single-octahedron clusters in the structure, which shows a very strong variation in different runs. This structure parameter is extremely sensitive to the element concentrations of Al and La. Although chemical analysis and refinement of the average structure were done with great care, the element concentrations could not be obtained with sufficient accuracy to allow reasonable determination of the concentration of single-octahedron clusters. This major shortcoming in the determination of the real structure is therefore a direct consequence of problems at steps usually done prior to the investigation of diffuse scattering. Obviously, small uncertainties in the average structure propagate to the real structure and may have a strong impact on the understanding of some aspects of the real structure. This finding strongly emphasizes the importance of determining the average structure as accurately as possible before starting the investigation of the disordered structure. Since diffuse scattering provides only information about *deviations from the average structure*, it can hardly compensate for uncertainties in the Bragg structure.

It can further be concluded that the combination of evolutionary algorithms with Monte Carlo modelling is capable of carrying out structure solution as well as refinement of a disorder model. In our study, model 2 is a typical example for a solution of the real structure, because it includes almost no *a priori* knowledge about the local structure. In analogy to well known average structure solution methods, the results obtained from model 2 give a quite reliable picture about the principles of the disordered structure. However, details are still to be refined using a more sophisticated model like model 1. Although not explicitly tested in this study, we currently see no clear indication that for the purposes of structure solution CE is superior to DE or *vice versa*. On the one hand, as the population is not required to converge, CE is more flexible and less prone to getting stuck in a local minimum, which is a welcome feature at the stage of structure solution. On the other hand, taking advantage of parallel computing is by far easier and more efficient when using DE. Thus, results may be obtained much faster and more variants may be tried out if large-scale computer clusters are available. For the purposes of structure refinement, however, DE is certainly the method of choice. The possibility of calculating population averages

does not only improve the accuracy of the results, but furthermore provides reasonable estimates about uncertainties. In the elitist-mode, standard deviations of population averages seem to underestimate uncertainties, while in the non-elitist mode uncertainties are overestimated. When using DE in elitist mode it was found that the best results regarding R values, structure parameters and estimates of uncertainties are obtained with a large mutation constant (0.8 in this study), while non-elitist-mode refinements show the best performance with small mutation constants (here 0.6). When carrying out CE refinements, uncertainties cannot be obtained from a single run, but have to be estimated by repeated refinements, which is extremely time consuming.

The calculations done in this study are computationally rather time consuming, and thus at present they do not seem to be attractive for the purposes of routine investigations. However, the problem addressed in this work is very demanding. The models not only have a relatively large number of parameters, but in addition the disorder problem is three-dimensional. This not only requires a complete three-dimensional experimental diffuse data set, but also refinement of three-dimensional disorder models. If experimental data show diffuse streaks or layers, as is frequently observed, then the disorder model is one- or two-dimensional as well, and structure simulation and calculation of the Fourier transform may be done by some orders of magnitude faster than in this study. Further, available computing power is still growing and evolutionary algorithms do not only benefit from faster CPUs, but in a quite natural way also from large-scale computer clusters and multi-processor architectures, which become more and more readily available. Finally, a better understanding of evolutionary algorithms in combination with Monte Carlo modelling, *e.g.* the role of population averaging, and the availability of more optimized computer code have a high potential for accelerating the investigations significantly.

We thank Professor Dr W. Schnick for generous support of this project.

References

Bürgi, H. B., Hauser, J., Weber, T. & Neder, R. B. (2005). *Cryst. Growth Des.* **5**, 2073–2083.

Butler, B. D. & Welberry, T. R. (1992). *J. Appl. Cryst.* **25**, 391–399.

Estermann, M. A. & Steurer, W. (1998). *Phase Transit.* **67**, 165–195.

Kienle, L., Oeckler, O., Weber, T., Duppel, V., Mattausch, Hj. & Simon, A. (2007). *Eur. J. Inorg. Chem.* pp. 1897–1902.

McGreevy, R. L. (2001). *J. Phys. Condens. Matter*, **13**, R877–R913.

Oeckler, O., Kienle, L., Mattausch, Hj., Jarchow, O. & Simon, A. (2003). *Z. Kristallogr.* **218**, 321–331.

Oeckler, O., Kienle, L., Mattausch, Hj. & Simon, A. (2002*a*). *Angew. Chem.* **114**, 4431–4433.

Oeckler, O., Kienle, L., Mattausch, Hj. & Simon, A. (2002*b*). *Angew. Chem. Int. Ed. Engl.* **41**, 4257–4259.

Oeckler, O., Mattausch, Hj. & Simon, A. (2005). *Z. Anorg. Allg. Chem.* **631**, 3013–3018.

Oeckler, O., Weber, T., Kienle, L., Mattausch, Hj. & Simon, A. (2005*a*). *Angew. Chem.* **117**, 3985–3989.

Oeckler, O., Weber, T., Kienle, L., Mattausch, Hj. & Simon, A. (2005*b*). *Angew. Chem. Int. Ed. Engl.* **44**, 3917–3921.

Proffen, Th. & Neder, R. B. (1997). *J. Appl. Cryst.* **30**, 171–175.

Proffen, Th. & Welberry, T. R. (1998). *Phase Transit.* **67**, 373–397.

Price, K. & Storn, R. (1997). *Dr. Dobb's J.*, April issue, pp. 18–24.

Ryazanov, M., Kremer, R. K., Simon, A. & Mattausch, Hj. (2006). *Phys. Rev. B*, **73**, 035114.

Simon, A. (1988*a*). *Angew. Chem.* **100**, 163–188.

Simon, A. (1988*b*). *Angew. Chem. Int. Ed. Engl.* **27**, 159–183.

Simon, A., Yoshiasa, A., Bäcker, M., Henn, R. W., Felser, C., Kremer, R. K. & Mattausch, Hj. (1996). *Z. Anorg. Allg. Chem.* **622**, 123–137.

Simon, A., Mattausch, Hj., Ryazanov, M. & Kremer, R. K. (2006). *Z. Anorg. Allg. Chem.* **632**, 919–929.

Stoe & Cie (1999). *XRED-32 1.03. Program for data handling*. Darmstadt, Germany.

Stoe & Cie (2002). *X-SHAPE 1.05. Program for crystal shape optimization for numerical absorption correction*. Based on the program *HABITUS* by W. Herrendorf, University of Giessen, Germany.

Weber, T. (2005). *Z. Kristallogr.* **220**, 1099–1107.

Weber, T. & Bürgi, H.-B. (2002). *Acta Cryst.* A**58**, 526–540.

Welberry, T. R. (2001). *Acta Cryst.* A**57**, 244–255.

Welberry, T. R. & Butler, B. D. (1994). *J. Appl. Cryst.* **27**, 205–231.

Welberry, T. R. & Goossens, D. J. (2008). *Acta Cryst.* A**64**, 23–32.

Welberry, T. R., Proffen, Th. & Bown, M. (1998). *Acta Cryst.* A**54**, 661–674.